

Efficient Neural Generation of 4K Masks for Homogeneous Diffusion Inpainting ^{*}

Karl Schrader¹, Pascal Peter¹, Niklas Kämper¹, and Joachim Weickert¹

Mathematical Image Analysis Group, Faculty of Mathematics and Computer Science,
Campus E1.7, Saarland University, 66041 Saarbrücken, Germany.
{schrader,peter,kaemper,weickert}@mia.uni-saarland.de

Abstract. With well-selected data, homogeneous diffusion inpainting can reconstruct images from sparse data with high quality. While 4K colour images of size 3840×2160 can already be inpainted in real time, optimising the known data for applications like image compression remains challenging: Widely used stochastic strategies can take days for a single 4K image. Recently, a first neural approach for this so-called mask optimisation problem offered high speed and good quality for small images. It trains a mask generation network with the help of a neural inpainting surrogate. However, these mask networks can only output masks for the resolution and mask density they were trained for. We solve these problems and enable mask optimisation for high-resolution images through a neuroexplicit coarse-to-fine strategy. Additionally, we improve the training and interpretability of mask networks by including a numerical inpainting solver directly into the network. This allows to generate masks for 4K images in around 0.6 seconds while exceeding the quality of stochastic methods on practically relevant densities. Compared to popular existing approaches, this is an acceleration of up to four orders of magnitude.

Keywords: Image Inpainting · Diffusion · Partial Differential Equations · Data Optimisation · Deep Learning.

1 Introduction

Inpainting-based image compression [12] is surprisingly simple: During encoding, only a carefully optimised subset of all pixel locations and their values is stored. In the decoding phase, the missing information is reconstructed in a lossy way by some inpainting method. Optimising the inpainting data, the so-called mask, is essential for obtaining a good reconstruction: Even with a simple method such as homogeneous diffusion inpainting [6], results can be surprisingly good.

Simple model-driven approaches for this optimisation problem require a compromise between reconstruction quality and speed [4,17]. Fast and qualitatively

^{*} This work has received funding from the European Research Council (ERC) under the European Union’s Horizon 2020 research and innovation programme (grant agreement no. 741215, ERC Advanced Grant INCOVID).

convincing results rely on sophisticated algorithms and implementations [7]. A first attempt to combine both advantages within a deep learning setting has been proposed recently by Alt et al. [2]. It is simple, fast, and approaches the quality of widely used model-driven optimisation strategies. It trains a mask generator network with the help of a neural inpainting surrogate. Extensions [21] allow to optimise not only the positions, but also the pixel values of the known data.

While offering a very good combination of quality and speed for greyscale images of sizes up to 256×256 and colour images up to 128×128 , it is inflexible: The mask network can only generate masks for the density and resolution it was trained for. Furthermore, a naïve extension to high-resolution images requires a prohibitive amounts of compute power during training: At a resolution of 3840×2160 , 4K colour images have around 25 million values, two to three orders of magnitude more than previously considered.

Our Contribution. With the first coarse-to-fine approach for neural mask generation, we address the weak points of the neural approach while preserving its high speed and increasing the quality of the generated masks. We partition the image into patches, and generate masks for each. Mask pixel budgets are assigned to each patch using an optimality result of Belhachmi et al. [4]. This constitutes the first transfer of their findings to the discrete setting which does not involve dithering, a step that usually leads to substantial quality losses. Our approach matches the quality of widely used stochastic mask optimisation strategies on 4K images of size 3840×2160 , while being up to four orders of magnitude faster. With a new training process, we solve the challenging problem of integrating model-based inpainting directly into the network. This removes the previous need for surrogate solvers and yields an overall more transparent and reliable architecture. Additionally, it greatly reduces the number of trainable weights and speeds up the training.

Related Work. There are many approaches for mask optimisation. The taxonomy below is an extension of the one of Peter et al. [21].

1. *Analytic Approaches.* For the continuous setting, Belhachmi et al. [4] were able to show that optimal masks can be derived from the Laplacian magnitude (modulus) of the image. To discretise this result, the Laplacian magnitude has been dithered so far. We apply this result in a novel way to estimate optimal patch densities in Section 4. Since analytic approaches do not require any inpaintings, they are very fast. However, dithering comes with significant compromises and typically results in low quality [17].
2. *Nonsmooth Optimisation Strategies.* Finding a good inpainting mask that minimises the mean squared error of the reconstruction can be phrased as a nonsmooth bilevel optimisation problem. It can be solved with primal-dual methods [5,14,18]. While being able to achieve high quality, they do not allow the user to specify a target density as for to our approach. In addition, they produce nonbinary masks and require binarisation as a postprocessing step which leads to a loss of quality. This can be alleviated by applying tonal optimisation [17], which optimises not only the position, but also the value

of the mask pixels. While this can introduce small errors to the known data, it is often beneficial for the overall quality of the reconstruction.

3. *Sparsification Methods*. This class of methods starts with a full mask and successively remove mask pixels with a low impact on reconstruction quality. One widely used implementation is *probabilistic sparsification* by Mainberger et al. [17]. It allows a target density to be specified and produces binary masks directly. However, it requires an inpainting to be computed in every step which results in long runtimes, especially on large images.
4. *Densification Methods*. They start with an empty mask and successively add those pixels to it which increase reconstruction quality the most [9,12]. Combined with ideas like finite elements [7], they constitute a fairly new but promising class of methods.
5. *Relocation Methods*. Greedy optimisation strategies can get stuck in local minima. To escape from them, *nonlocal pixel exchange* [17] tests if moving some randomly selected mask pixels into the unknown regions leads to a better reconstruction. Successful moves are kept, while unsuccessful ones are reverted. Given sufficient time, this method can produce very good masks. It is usually applied as a postprocessing tool.
6. *Neural Methods*. Works such as [8,20] learn the inpainting operator along with a mask generation network. As this results in an opaque model, we focus on well-understood homogeneous diffusion inpainting. For it, [2,21] have shown that a mask generation network can be successfully trained with the help of an inpainting surrogate, but focus on small images of sizes up to 256×256 . Opposed to our model, new densities and resolutions require a new model to be trained. Their framework also allows for the training of a tonal optimisation network with the same strategy. While this is also the case for our approach, we focus on the spatial case due to space limitations. Inference with neural mask generation is very fast since it requires no inpaintings.

These approaches can be summarised as follows: Category 1 is very fast as it requires no inpaintings, but offers low quality. Higher quality is achieved by Categories 2 – 4 at the expense of speed, as they all need to calculate many inpaintings. Given sufficient iterations, Category 5 can improve any mask further. Previous neural methods from Category 6 offer good quality and speed, but are not as flexible as model-driven approaches. We will exploit optimality results from Category 1 without sacrificing quality through dithering to alleviate the shortcomings of Category 6.

Organisation of the Paper. Section 2 reviews inpainting with homogeneous diffusion and model-driven spatial optimisation. Section 3 presents our improvements to the baseline neural mask generation architecture, followed by our new coarse-to-fine mask generation strategy in Section 4. Section 5 provides empirical evidence for our patch density estimation and compares our neural approach against model-driven ones. We end with conclusions and an outlook in Section 6.

2 Homogeneous Diffusion Inpainting

Let us consider a continuous greyscale image $f : \Omega \rightarrow \mathbb{R}$ defined on a rectangular image domain Ω which is only known on a mask $K \subset \Omega$. The goal of inpainting is to restore the inpainting region $\Omega \setminus K$ with a homogeneous diffusion process that propagates information; see e.g. [13]. For homogeneous diffusion inpainting [6], the reconstruction solves the partial differential equation

$$(1 - c)\Delta u - c(u - f) = 0 \quad (1)$$

where $c : \Omega \rightarrow \{0, 1\}$ is a binary confidence function which indicates if a point \mathbf{x} is part of the mask. Known values are specified by $c(\mathbf{x}) = 1$ and are preserved. Missing data are indicated by $c(\mathbf{x}) = 0$ and are inpainted with the steady state $\Delta u = 0$ of the homogeneous diffusion equation, where $\Delta = \partial_{xx} + \partial_{yy}$ is the Laplacian. We assume reflecting boundary conditions at the image boundary $\partial\Omega$. Nonbinary masks are also well-defined within the mathematical framework, but are hard to compress and only used as an intermediate step in this work. For colour images, each channel is considered independently, since homogeneous diffusion is a linear operator.

While more sophisticated inpainting models exist [12,23], homogeneous diffusion is attractive for inpainting-based compression: Its simplicity allows for an analytic continuous theory for inpainting data selection [4] and enables fast implementations [15]. Furthermore, its complete lack of parameters make it easy to use, and it can yield high-quality reconstruction for well optimised inpainting data. These properties make it a suitable candidate for mask optimisation.

In the discrete setting, we consider digital colour images $\mathbf{f} \in \mathbb{R}^{3n_x n_y}$ with resolution $n_x \times n_y$. The inpainting equation (1) is discretised with finite differences, leading to a linear system of equations. The reconstruction \mathbf{u} can then be computed by a suitable numerical solver such as the conjugate gradient method; see e.g. [24]. Mask optimisation strategies are designed to generate discrete masks $\mathbf{c} \in \{0, 1\}^{n_x n_y}$ such that the corresponding reconstruction \mathbf{u} approximates the original image well. They are constrained by the mask density $\|\mathbf{c}\|_1 / (n_x n_y)$ where $\|\cdot\|_1$ is the 1-norm, which should match the desired target density d .

2.1 Model-Based Mask Optimisation

A mask optimisation strategy that does not require any inpaintings has been proposed by Bellhachmi et al. [4]. They show that for optimal masks, the local density should increase with the Laplacian magnitude. In Section 4 we use this result to predict a suitable density for image regions. However, the application of these results to discrete images relies on dithering. The commonly used Floyd-Steinberg dithering [11] is fast and simple, but suffers from a directional bias and generates masks of relatively low quality.

A method which produces better masks but remains simple is *probabilistic sparsification* [17]. It starts with a full mask and gradually removes pixels until

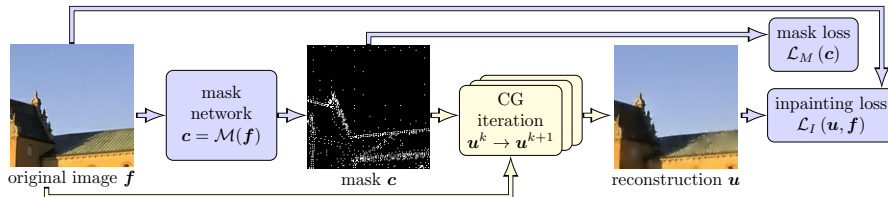


Fig. 1. Our Mask Optimisation Architecture. The mask network and its losses are coloured in blue, our newly introduced sequence of CG iterations is given in yellow.

the target density d is reached. In every iteration, a fraction p of mask pixels is removed. Then, an inpainting is computed, and the fraction q which resulted in the largest loss of quality is added back.

We also consider *nonlocal pixel exchange* [17] as a post-processing method. In each step, it moves a fraction p of mask pixels into the unknown image area. It then inpaints with the new mask to check for improvements: Exchanges which increase inpainting quality are kept, while unsuccessful ones are reverted. This is repeated for k cycles with $\|c\|_1$ iterations each. Nonlocal pixel exchange can help greedy approaches like probabilistic sparsification escape from poor local minima at the cost of significant runtime.

Both probabilistic sparsification and nonlocal pixel exchange require an inpainting for each iteration, with the other operations being quick in comparison. As such, their runtime is primarily determined by the number and the speed of the inpainting operations. A naïve CPU-based inpainter using a conjugate gradient solver takes around 3.5 seconds per 4K colour image on a contemporary PC. At this speed, 5 cycles of nonlocal pixel exchange for a mask with 5% known data would take around 12 weeks. To enable meaningful comparisons, we have developed implementations of probabilistic sparsification and nonlocal pixel exchange that use the very fast GPU-based inpainting of Kämper et al. [15]. With it, an iteration of either method requires only ≈ 6 milliseconds, a speedup of two orders of magnitude. To the best of our knowledge, our implementations are the fastest available.

3 Neural Mask Generation

We follow the basic network architecture from Peter et al. [21] with a mask generator network and an inpainting approximator. The latter is used to train the mask network by evaluating the reconstruction quality and is discarded during inference. An overview of our architecture can be found in Figure 1. While we retain the mask network as is, we completely replace the original inpainting approximator.

Mask Network. The mask network receives the original image f and generates a mask $c = \mathcal{M}(f)$. Its output is restricted to $[0, 1]$ by applying a sigmoid activation function. Additionally, the network outputs are rescaled if they exceed

the desired density d . The goal of the network is to produce masks such that the corresponding inpainted image \mathbf{u} is close to the original \mathbf{f} . To this end, we minimise their mean squared error (MSE) $\mathcal{L}_I(\mathbf{u}, \mathbf{f}) = \frac{1}{n_x n_y} \|\mathbf{u} - \mathbf{f}\|_2^2$ where $\|\cdot\|_2$ is the Euclidean norm. In addition, we require a mechanism to encourage the generation of binary masks. To this end, we penalise the inverse variance of the mask using $\mathcal{L}_M(\mathbf{c}) = \alpha(\sigma_c^2 + \varepsilon)^{-1}$ where ε is a small numerical constant to avoid division by 0, and α balances variance loss \mathcal{L}_M and inpainting loss \mathcal{L}_I .

Inpainting Approximator. To train the mask network with an inpainting loss \mathcal{L}_I , we need to approximate the inpainting process inside the network. Previous approaches [2,21] facilitate this by including a surrogate inpainting network which receives the original \mathbf{f} and mask \mathbf{c} , and is trained to find a reconstruction \mathbf{u} which solves the discrete version of the inpainting equation (1):

$$(\mathbf{I} - \mathbf{C})\mathbf{A}\mathbf{u} - \mathbf{C}(\mathbf{u} - \mathbf{f}) = \mathbf{0} \quad (2)$$

Here, the matrix $\mathbf{C} = \text{diag}(\mathbf{c})$ contains the mask entries on the diagonal, and \mathbf{A} applies a finite difference discretisation of the Laplacian Δ with reflecting boundary conditions. This approach significantly increases the total number of weights and adds complexity to the architecture. Furthermore, it decreases interpretability as the surrogate is, apart from its loss function, a black box.

We propose to replace it by a sufficient number of iterations of a successful numerical solver. As homogeneous diffusion leads to a linear system of equations with a symmetric system matrix, we can use the conjugate gradient (CG) method [24]. It offers convergence guarantees while remaining simple and efficient. As each iteration is differentiable, we can backpropagate through the solver to train the mask network. By introducing this well-understood numerical solver, we have reduced the total number of weights by half compared to [21] while increasing interpretability. Section 5.2 confirms that this improves inpainting approximation quality greatly and the quality of generated masks slightly.

Mask Generation in Practice. As the generated masks are not guaranteed to be binary, we need to binarise them. To this end, Peter et al. [21] perform weighted coinflips at each mask pixel and then choose the best-performing mask out of 30 attempts. We found that rounding leads to a comparable quality for our masks. It is less time intensive and involves no randomness.

4 Coarse-To-Fine Approach for Mask Generation

Simply partitioning a large image into patches and generating masks with equal density for each leads to suboptimal results: Textured regions receive too few, while homogeneous areas receive too many mask pixels. As such, we require a fast and simple mechanism that estimates suitable densities for each patch while taking the whole image into account.

To this end, we estimate a good patch density using the average Laplacian magnitude per patch, similar to the approach by Belhachmi et al. [4]. They

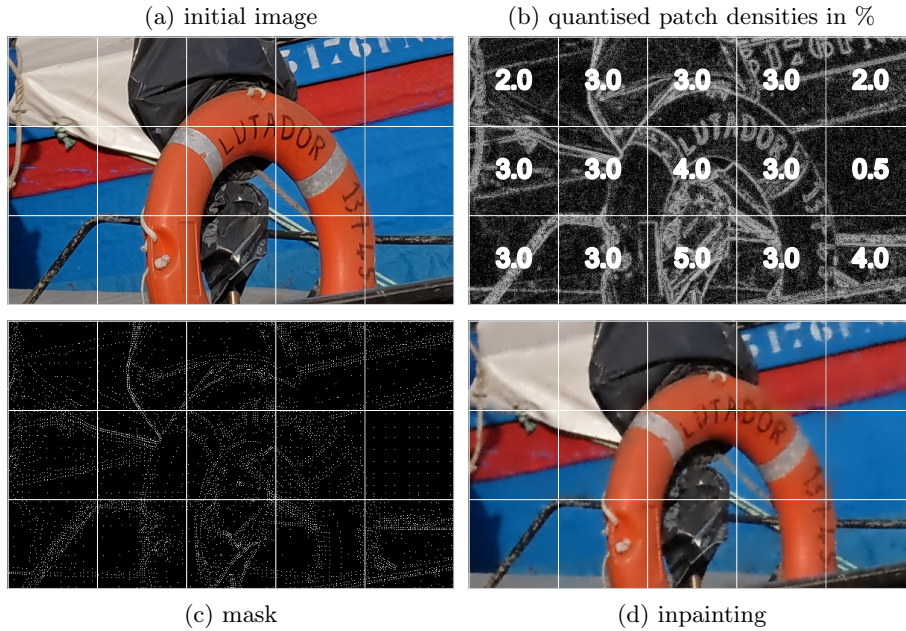


Fig. 2. Stages of the Mask Generation Process. (a) Initial image with subdivision into patches. (b) Quantised patch densities, and Laplacian magnitude with logarithmic dynamic compression for better visibility in the background. (c) Binary mask with 3% known data. (d) Inpainted result.

have shown that for optimal continuous masks, the local mask density should increase with the Laplacian magnitude. The discrete approximation of this result through dithering requires significant compromises. We, however, aggregate the Laplacian magnitude over an image patch to estimate the optimal density and thus avoid dithering completely. To the best of our knowledge, we are the first to apply the optimality result this way. This motivates the following algorithm, which is also visualised in Figure 2:

1. Compute the Laplacian magnitude of the luma channel for every pixel.
2. Rescale it such that its global mean matches the target density.
3. Compute the target patch densities as the mean of the rescaled Laplacian magnitude per patch. Section 5.2 confirms that these target densities correlate well with high-quality masks.
4. Quantise the patch densities to values for which pre-trained mask networks are available and generate masks for every patch.
5. Assemble the mask patches into a mask for the whole image.

As an additional benefit, this methodology allows to generate masks with arbitrary densities. This is achieved by selecting densities per patch out of the available ones such that their mean approximates the desired average well.



Fig. 3. Our 12 test images of size 3840×2160 . Photos by J. Weickert.

5 Experiments

After mentioning the technical details in Section 5.1, we show the improvements made by introducing a CG solver into the network in Section 5.2. Additionally, we provide empirical evidence for our patch density estimation in Section 5.3, and compare the mask generation performance for 4K images in Section 5.4.

5.1 Experimental Setup

For our mask generator, we use the same small multiscale context aggregation network [22] with ≈ 2.9 million parameters and settings as in [21] to facilitate direct comparisons. It is based on a U-Net architecture with four scales and uses blocks of parallel dilated convolutions with different dilation rates. All mask networks are trained with the losses described in Section 3. The mask variance loss weight is set to $\alpha = 0.01$. The surrogate network in Section 5.2 shares the mask network architecture and uses the squared residual of the discrete inpainting equation (2) as its loss. All networks are trained for 100 epochs with a batch size of 8 and the Adam optimiser [16] with a learning rate of $5 \cdot 10^{-5}$. Performance is evaluated on an AMD Ryzen 7 5800X CPU and an Nvidia RTX 3090 GPU. For comparisons against [21], we trained on a subset of 100,000 images from ImageNet [10] sampled by Dai et al. [8]. Tests are performed on

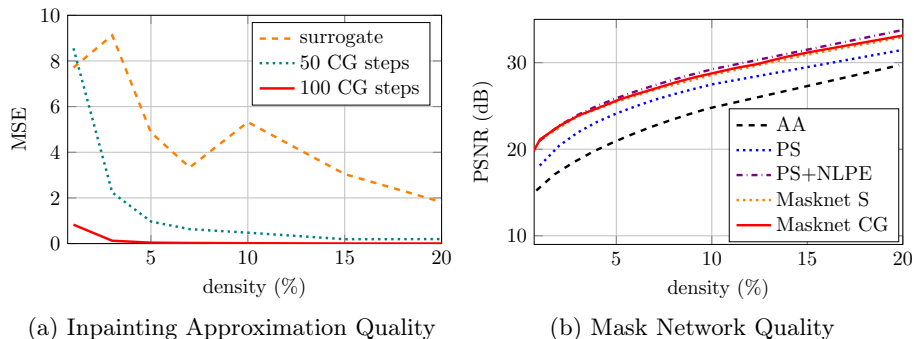


Fig. 4. Comparison of Different Inpainting Approximators. (a) Distance between the inpainting approximations and a converged inpainting. The MSEs decrease in a nonmonotone fashion due to the varying quality of different mask and inpainting networks. (b) Comparison of mask networks trained with either a surrogate inpainter (Masknet S) or 100 CG iterations (Masknet CG). Even though 100 CG iterations are a much better inpainting approximator, the quality of the mask network trained with them is only slightly improved. Both methods are better than the analytic approach (AA) and probabilistic sparsification (PS), and are very close to PS with added nonlocal pixel exchange (PS+NLPE).

the full BSDS500 dataset [3]. We used 128×128 centre crops for both. The networks used for 4K inpainting were trained on 100,000 random patches of size 120×120 from the high-resolution image dataset Div2K [1]. Tests are performed on 12 representative 4K images photographed by one of the authors; see Figure 3. Our selection of pre-trained networks is optimised for target densities $\leq 10\%$, as those are practically relevant for compression. The set contains networks for different densities in the range from 0.5% to 80%. For 1%-15%, we use increments of 1%. For 15%-25% we increment by 2%, and by 5% for densities between 25% and 50%. Finally, in the range of 50%-80% we have steps of 10%. Reference inpaintings are computed using a CG solver which is stopped after a relative decrease of the Euclidean norm of the residual of 10^{-6} .

For comparisons against model-driven approaches, we use the analytic approach (AA) by Belhachmi et al. [4], and probabilistic sparsification (PS) alone or combined with nonlocal pixel exchange (PS+NLPE). PS uses candidate fractions $p = 0.3$ and $q = 0.005$. NLPE runs for 5 cycles. The other NLPE parameters were optimised individually for the different target resolutions.

5.2 Quality of Inpainting Approximations

We measure the quality of different inpainting approximators by comparing against inpaintings with our reference solver. To avoid a bias against the surrogate inpainting networks, we test on binarised masks generated by their corresponding mask networks. In Figure 4(a), we see that 100 CG iterations are a

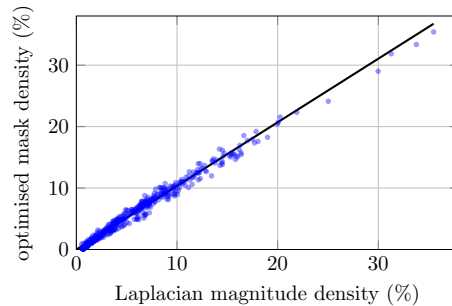


Fig. 5. Patch Density Correlation between Laplacian Magnitude and High Quality Mask. Comparison of the mean rescaled Laplacian magnitude for each patch of the image *lofsdalen* against patch densities of a high quality mask, both with a total density of 5%. A correlation coefficient of 0.994 confirms the strong connection.

better approximator than the surrogate network across all densities. Additionally, they allow for faster training: On image batches, one forward and backward pass takes only 1.9 ms per image, while the surrogate requires 5.6 ms. Nevertheless, the quality of the trained mask network is only slightly improved by using CG as an inpainting approximator as can be seen in Figure 4(b). This makes sense as the reconstruction error is about 3000 times larger than the approximation error for 100 CG steps and all densities, making small deviations insignificant.

5.3 Justification of Mask Pixel Distribution

In Figure 5 we show that the rescaled Laplacian magnitude is a good predictor of optimal mask densities at a patch level. There we compare against the patch densities of a well optimised mask generated with the approach from Chizhov and Weickert [7]. The relationship between the patch densities is almost linear, and the mean absolute error between densities is only 0.5%. While dithering the rescaled Laplacian magnitude leads to low-quality masks, its aggregation over a patch avoids this and produces a good coarse scale density estimate.

5.4 High-Resolution Mask Generation

The tests on 4K images in Figure 6(a) show that our masknet trained with 100 CG iteration is superior to AA and PS for all densities. In addition, we are even able to outperform PS+NLPE on densities smaller than 8%. This range is practically relevant for inpainting-based compression.

In Figure 6(b) we compare the speed of the different methods. The runtime of PS+NLPE scales with the required inpaintings, taking between 30 minutes and 8.5 hours depending on the density. In contrast, our neural approach takes only about 0.6 seconds per image. It is even quicker for the lowest densities

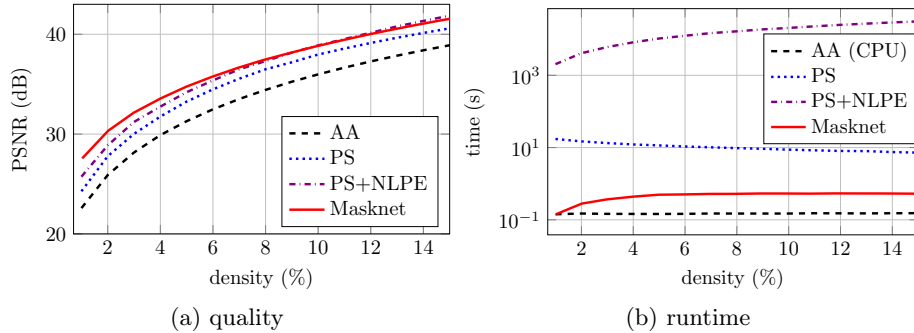


Fig. 6. Spatial Optimisation. Our masknet outperforms the faster analytic approach, but also the slower PS across all densities. It even beats the significantly slower PS+NLPE for densities $\leq 8\%$. Time measurements exclude input/output operations.

where fewer of the pre-trained mask networks are active and the batches per net are larger. Our masknet is also more than 10 times faster than the qualitatively worse PS. The analytic approach requires no inpaintings, and even a CPU-based implementation is significantly faster than our neural method. Still, its quality is inferior by a large margin. In Figure 7, the most noticeable differences are slightly blurry edges for AA, and a discoloured sky for PS and PS+NLPE.

6 Conclusions

Our coarse-to-fine approach for mask generation is orders of magnitude faster than qualitatively similar approaches on 4K images. This shows that the estimation of patch densities using the optimality result by Belhachmi et al. [4] works well, and our mask networks are able to outperform dithering. Performance of the neural approach relative to PS+NLPE even grew with the increase in resolution. Our experiments suggest that the coarse-to-fine approach produces local problems that are easier and faster to solve in high quality. This is in line with transform-based codecs like JPEG [19], which also use a block structure to enable parallelisation and reduce complexity.

In the future, we will investigate these coarse-to-fine approaches for mask generation further using various local solvers. This avenue of research becomes even more desirable given the ever-increasing parallelisation capabilities of modern GPUs, rapidly increasing image resolutions, and the fact that reasonably simple solvers such as CG cannot offer optimal linear complexity.

References

- Agustsson, E., Timofte, R.: NTIRE 2017 challenge on single image super-resolution: Dataset and study. In: Proc. 2017 IEEE Computer Society Conference on Computer Vision and Pattern Recognition Workshops. vol. 1, pp. 1122–1131. Honolulu, HI (Jul 2017)

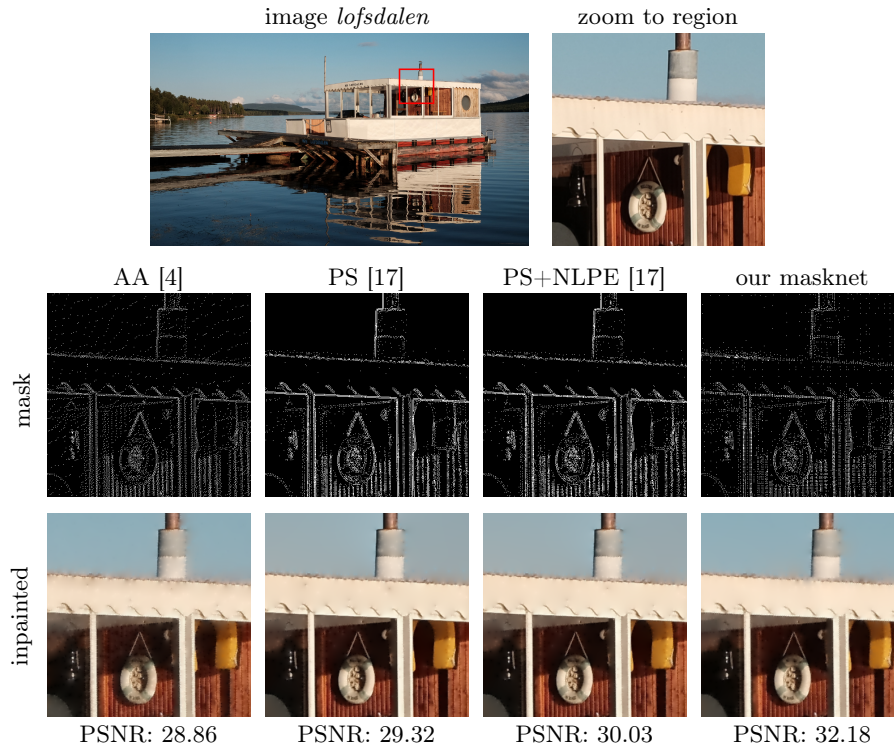


Fig. 7. Visual Comparison for 4% Mask Density on *lofsdalen*. PSNRs are for the whole image. Notice the discoloured sky for PS and PS+NLPE. The full images are available in the supplementary material.

2. Alt, T., Peter, P., Weickert, J.: Learning sparse masks for diffusion-based image inpainting. In: Pinho, A.J., Georgieva, P., Teixeira, L.F., Sánchez, J.A. (eds.) Pattern Recognition and Image Analysis, Lecture Notes in Computer Science, vol. 13256, pp. 528–239. Springer, Cham (2022)
3. Arbelaez, P., Maire, M., Fowlkes, C., Malik, J.: Contour detection and hierarchical image segmentation. *IEEE Transactions on Pattern Analysis and Machine Intelligence* **33**(5), 898–916 (Aug 2011)
4. Belhachmi, Z., Bucur, D., Burgeth, B., Weickert, J.: How to choose interpolation data in images. *SIAM Journal on Applied Mathematics* **70**(1), 333–352 (2009)
5. Bonettini, S., Loris, I., Porta, F., Prato, M., Rebegoldi, S.: On the convergence of a linesearch based proximal-gradient method for nonconvex optimization. *Inverse Problems* **33**(5), Article no. 055005 (Mar 2017)
6. Carlsson, S.: Sketch based coding of grey level images. *Signal Processing* **15**, 57–83 (1988)
7. Chizhov, V., Weickert, J.: Efficient data optimisation for harmonic inpainting with finite elements. In: Tsapatsoulis, N., Panayides, A., Theodorides, T., Lanitis, A., Pattichis, C., Vento, M. (eds.) Computer Analysis of Images and Patterns. Part 2., Lecture Notes in Computer Science, vol. 13053, pp. 432–441. Springer, Cham (2021)

8. Dai, Q., Chopp, H., Pouyet, E., Cossairt, O., Walton, M., Katsaggelos, A.K.: Adaptive image sampling using deep learning and its application on X-ray fluorescence image reconstruction. *IEEE Transactions on Multimedia* **22**(10), 2564–2578 (Dec 2019)
9. Daropoulos, V., Augustin, M., Weickert, J.: Sparse inpainting with smoothed particle hydrodynamics. *SIAM Journal on Applied Mathematics* **14**(4), 1669–1704 (Nov 2021)
10. Deng, J., Dong, W., Socher, R., Li, L.J., Li, K., Fei-Fei, L.: Imagenet: A large-scale hierarchical image database. In: *Proc. 2009 IEEE Computer Society Conference on Computer Vision and Pattern Recognition*. pp. 248–255. Miami, FL (Aug 2009)
11. Floyd, R.W., Steinberg, L.: An adaptive algorithm for spatial grey scale. *Proceedings of the Society of Information Display* **17**, 75–77 (1976)
12. Galić, I., Weickert, J., Welk, M., Bruhn, A., Belyaev, A., Seidel, H.P.: Image compression with anisotropic diffusion. *Journal of Mathematical Imaging and Vision* **31**(2–3), 255–269 (Jul 2008)
13. Guillemot, C., Le Meur, O.: Image inpainting: Overview and recent advances. *IEEE Signal Processing Magazine* **31**(1), 127–144 (2014)
14. Hoeltgen, L., Setzer, S., Weickert, J.: An optimal control approach to find sparse data for Laplace interpolation. In: Heyden, A., Kahl, F., Olsson, C., Oskarsson, M., Tai, X.C. (eds.) *Energy Minimisation Methods in Computer Vision and Pattern Recognition*, *Lecture Notes in Computer Science*, vol. 8081, pp. 151–164. Springer, Berlin (2013)
15. Kämper, N., Weickert, J.: Domain decomposition algorithms for real-time homogeneous diffusion inpainting in 4K. In: *Proc. 2022 IEEE International Conference on Acoustics, Speech and Signal Processing*. pp. 1680–1684. Singapore (May 2022)
16. Kingma, D.P., Ba, J.: Adam: A method for stochastic optimization. In: *Proc. 3rd International Conference on Learning Representations*. San Diego, CA (May 2015)
17. Mainberger, M., Hoffmann, S., Weickert, J., Tang, C.H., Johannsen, D., Neumann, F., Doerr, B.: Optimising spatial and tonal data for homogeneous diffusion inpainting. In: Bruckstein, A.M., ter Haar Romeny, B., Bronstein, A.M., Bronstein, M.M. (eds.) *Scale Space and Variational Methods in Computer Vision*, *Lecture Notes in Computer Science*, vol. 6667, pp. 26–37. Springer, Berlin (2012)
18. Ochs, P., Chen, Y., Brox, T., Pock, T.: iPiano: Inertial proximal algorithm for non-convex optimization. *SIAM Journal on Imaging Sciences* **7**(2), 1388–1419 (2014)
19. Pennebaker, W.B., Mitchell, J.L.: *JPEG: Still Image Data Compression Standard*. Springer, New York (1992)
20. Peter, P.: A Wasserstein GAN for joint learning of inpainting and its spatial optimisation. *arXiv:2202.05623 [eess.IV]* (Feb 2022)
21. Peter, P., Schrader, K., Alt, T., Weickert, J.: Deep spatial and tonal data optimisation for homogeneous diffusion inpainting. *arXiv:2208.14371 [eess.IV]* (Aug 2022)
22. Vařata, D., Halama, T., Friedjungová, M.: Image inpainting using Wasserstein generative adversarial imputation network. In: Farkaš, I., Masulli, P., Otte, S., Wermter, S. (eds.) *Artificial Neural Networks and Machine Learning – ICANN 2021*, *Lecture Notes in Computer Science*, vol. 12892, pp. 575–586. Springer, Cham (2021)
23. Weickert, J., Welk, M.: Tensor field interpolation with PDEs. In: Weickert, J., Hagen, H. (eds.) *Visualization and Processing of Tensor Fields*, pp. 315–325. Springer, Berlin (2006)
24. Wendland, H.: *Numerical Linear Algebra: An Introduction*. Cambridge University Press, Cambridge, MA (Nov 2017)